Analysis of Steady-State Error in Torque Current Component Control of PMSM Drive

Pavel BRANDSTETTER, Ivo NEBORAK, Martin KUCHAR

Department of Electronics, VSB-Technical University of Ostrava, 70833, Czech Republic

pavel.brandstetter@vsb.cz

Abstract—**The paper presents dynamic properties of a vector controlled permanent magnet synchronous motor drive supplied by a voltage source inverter. The paper deals with a control loop for the torque producing stator current. There is shown fundamental mathematical description for the vector control structure of the permanent magnet synchronous motor drive with respect to the current control for *d*-axis and *q*-axis of the rotor rotating coordinate system. The derivations of steady-state deviation for schemes with and without decoupling circuits are described for *q*-axis. The properties of both schemes are verified by MATLAB-SIMULINK program considering a lower and a higher value of inertia and by experimental measurements in our laboratory. The simulation and experimental results are presented and discussed at the end of the paper.**

Index Terms—**AC motors, electric current control, machine vector control, permanent magnet motors, variable speed drives.**

I. Introduction

At present, the importance of variable speed electrical drives with permanent magnet synchronous motors (PMSM) is growing [1-5]. The magnetic flux and the torque may be controlled by vector control [6, 7], or by direct torque control [8-11]. Current research activities of scientific institutions include a sensorless control of the PMSM drives that uses different rotor speed estimation methods [12-17]. Modern analysis and design methodology of the PMSM enable new construction solutions of the PMSM [18, 19].

In general, it is known that a current control of DC or AC drives has a steady-state error. If the current control loop is designed as the subordinate loop of the speed or position control, the steady-state current error is not such a big problem and it leads to worse dynamic performance of the electric drive. Different situation is for a torque or current control without a superordinate loop, e.g. a torque control of electric drives for robotics or traction applications. In these cases, it is necessary to eliminate or at least to increase the admissible value of the current control error [20-30].

For the vector controlled PMSM, there are very often used circuits to cancel the coupling between flux and torque producing components of the stator current vector. This coupling occurs in the voltage equations expressed in the rotating reference frame for *d*-axis and *q*-axis. It is known that the decoupling circuits are necessary for the independent control of both current components of the stator current vector, but in this paper there is shown and verified that the

decoupling circuits eliminate the steady-state error of torque producing stator current control too.

II. Mathematical Model of the Vector Controlled Permanent Magnet Synchronous Motor

For assembling a mathematical model of the PMSM, we can use theory of a general AC machine. Given that the excitation magnetic flux of the rotor is generated by the permanent magnets, for describing the properties of the machine and for the vector control it is suitable to choose as reference the $[d, q]$ rotating coordinate system. The magnetic flux generated by the permanent magnets induces in the stator winding a voltage during rotation of the PMSM rotor.

The vector control of the PMSM uses a principle of stator current vector components separation. These current components i_{Sd} and i_{Sq} are orthogonal and influence a magnetization and torque of the PMSM.

The *d*-axis of the $[d, q]$ rotating coordinate system is determined by the position of the magnetic flux vector created by permanent magnets Φ_F (Fig. 1).
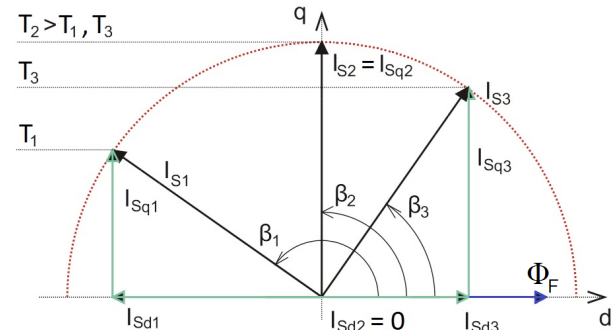

Figure 1. Stator current vector components in different regimes

For the stator voltage vector components in the $[d, q]$ rotor rotating coordinate system, there are valid the following voltage equations:

$$u_{Sd} = R_S i_{Sd} + \frac{d\Psi_{Sd}}{dt} - \omega\Psi_{Sq} =$$
$$= R_S i_{Sd} + \frac{d(L_{Sd}i_{Sd} + \Phi_F)}{dt} - \omega L_{Sq}i_{Sq} = \qquad (1)$$
$$= R_S i_{Sd} + L_{Sd}\frac{di_{Sd}}{dt} - \omega L_{Sq}i_{Sq} \ ,$$

$$u_{Sq} = R_S i_{Sq} + \frac{d\Psi_{Sq}}{dt} + \omega\Psi_{Sd} = R_S i_{Sq} + L_{Sq}\frac{di_{Sq}}{dt} + \qquad (2)$$
$$+ \omega(L_{Sd}i_{Sd} + \Phi_F) \ ,$$

where: i_{Sd}, i_{Sq} – stator current vector components in $[d, q]$ rotating coordinate system; u_{Sd}, u_{Sq}– stator voltage vector

components in $[d, q]$ rotating coordinate system; Φ_F— magnetic flux of permanent magnets; L_{Sd} – stator inductance in d-axis; L_{Sq} – stator inductance in q-axis; R_S– stator phase resistance; ω – electrical angular speed of the rotor; Θ– rotor angle.

The PMSM torque is defined as follows:

$$T = \frac{3}{2} p \left[\Phi_F + \left(L_{Sd} - L_{Sq} \right) i_{Sd} \right] i_{Sq} . \tag{3}$$

For a Surface PMSM, $L_{Sd} \approx L_{Sq}$, and then Eq. (3) will have the form:

$$T = \frac{3}{2} p \; \Phi_F i_{Sq} . \tag{4}$$

The motion equation is:

$$T - T_L = J_t \frac{d\Omega_m}{dt} , \tag{5}$$

where: J_t – inertia; p – number of pole pairs; T – PMSM torque; T_L – load torque; Ω_m – mechanical rotor angular speed.

The electrical rotor speed is given by the derivative of the electrical rotor angle:

$$\omega = p \; \Omega_m = \frac{d\Theta}{dt} , \tag{6}$$

Electromagnetic time constants in d-axis and q-axis are defined by following equations:

$$T_{Sd} = \frac{L_{Sd}}{R_S} , \tag{7}$$

$$T_{Sq} = \frac{L_{Sq}}{R_S} . \tag{8}$$

From voltage Eqs. (1) and (2), we obtain the equations for the current components that are important for further analysis. After Laplace transformation, we obtained the following relationships for the d- and q-components of the stator current vector.

$$i_{Sd} = \frac{1}{R_S \left(1 + sT_{Sd} \right)} \left[u_{Sd} + \omega L_{Sq} i_{Sq} \right] , \tag{9}$$

$$i_{Sq} = \frac{1}{R_S \left(1 + sT_{Sq} \right)} \left[u_{Sq} - \omega \left(\Phi_F + L_{Sd} i_{Sd} \right) \right] . \tag{10}$$

The square brackets in Eqs. (9) and (10) contain terms that represent the undesirable coupling between d and q components.

III. Control Structure of the PMSM Drive

The speed control structure of the permanent magnet synchronous motor drive with the vector control is shown in Fig. 2. The control structure is formed by so-called subordinate control loops that consist of one or more simple controllers. In Fig. 2, the following blocks were used:

SM – synchronous motor;
FC – frequency converter;
T 3/2 – block of the Clarke transformation;
PWM – block of the pulse-width modulation;
ESP – block of the position estimation;
CS – current sensors;
DEC – block of the decoupling of d- and q-axes;
$e^{j\Theta}$, $e^{-j\Theta}$ – blocks for rotation of vectors;
TAB – block for calculating the sin/cos functions.

In the sensorless control technique, a position or speed estimator which uses different types of estimation methods is used. We used a position sensor PS for the estimation of the rotor angle Θ.
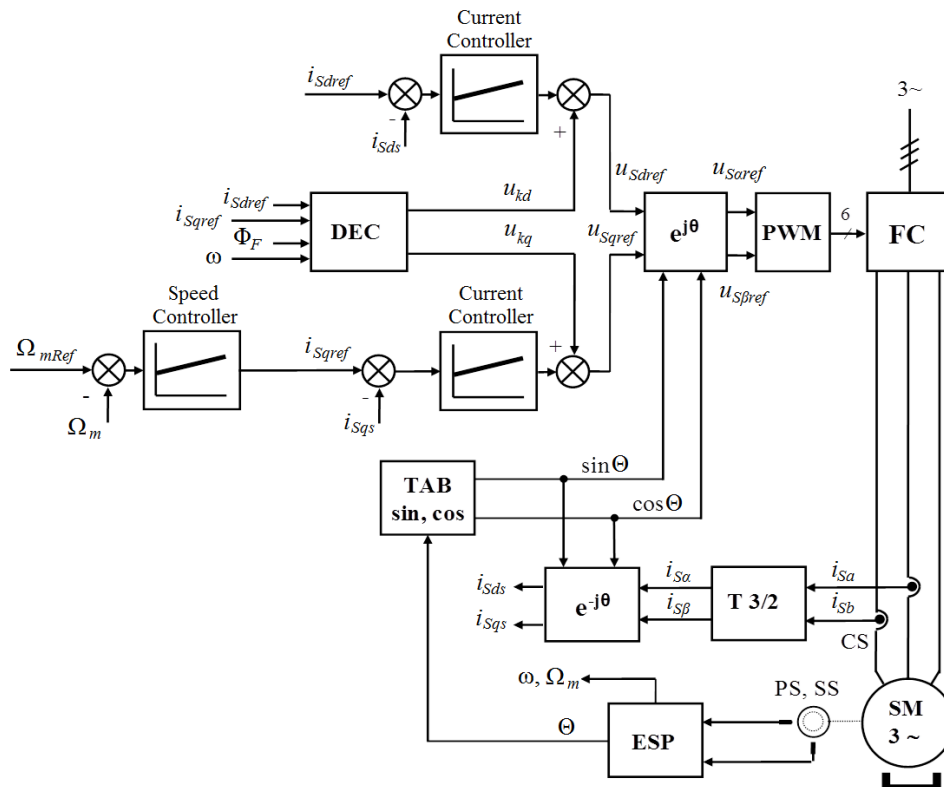

Figure 2. Speed control structure of the vector controlled AC drive with the PMSM

The vector rotation and the reverse vector rotation of the complex space vector components from the [α, β] stationary coordinate system to the [d, q] rotor rotating coordinate system respectively, are performed using the rotor angle Θ.

The stator current component i_{SdRef} that produces the reference flux is zero for a speed up the nominal value Ω_{mN}. Above this value of the speed, this component of the stator current decreases to negative values according to the actual value of the speed Ω_m. This is the so-called field weakening of the PMSM.

The stator current component i_{SdRef} that produces the reference torque is determined by the PI speed controller.

Both components of the stator current vector are then controlled in subordinate current control loops.

On the basis of previous equations, it can be drawn a current control block scheme of the vector controlled PMSM without decoupling (Fig. 3).

Fig. 3 consists of the following transfer functions:

F_{CCd} – transfer function of the current controller in *d*-axis;
F_{CCq} – transfer function of the current controller in *q*-axis;
F_{FC} – transfer function of the frequency converter;
F_{CS} – transfer function of the current sensor.

Fig. 3 describes the coupling between the stator current component i_{Sd} that produces the magnetizing current and the stator current component i_{Sq} that produces the torque, necessary for the vector control of the PMSM.

The coupling cancellation, that we called decoupling, can be made using members whose output signals are added to output signals of the current controllers.

The voltage components u_{kd} and u_{kq} are added to the output voltage signals of the current controllers to eliminate the coupling between *d*-axis and *q*-axis according to (11) and (12). These components are determined in block of decoupling DEC (Fig. 2).

The decoupling is performed using the following equations:

$$u_{kd} = -\omega L_{Sq} i_{Sq} \quad , \tag{11}$$

$$u_{kq} = \omega \left(\Phi_F + L_{Sd} i_{Sd} \right) \quad . \tag{12}$$

The Chapter IV deals with the torque current component control only. For the analysis of the decoupling influence, it is considered an activity of the PMSM drive in the speed range to the nominal speed ($i_{Sd} = 0$).

IV. PARAMETERS OF PMSM DRIVE

For the analysis of the steady-state error of the torque current component, the PMSM drive from the laboratory of the Department of Electronics, Technical University of Ostrava is considered.

In Table I, the main parameters of the used Surface PMSM with rare earth PM type 1FK 7063-5AF71 (Siemens) are shown. The induced voltage is approximately sinusoidal. The PMSM is loaded by an induction machine. The inertia of the PMSM drive is J_t=31.1·10⁻⁴ kgm².

TABLE I. PARAMETERS OF SURFACE-MOUNTED PMSM

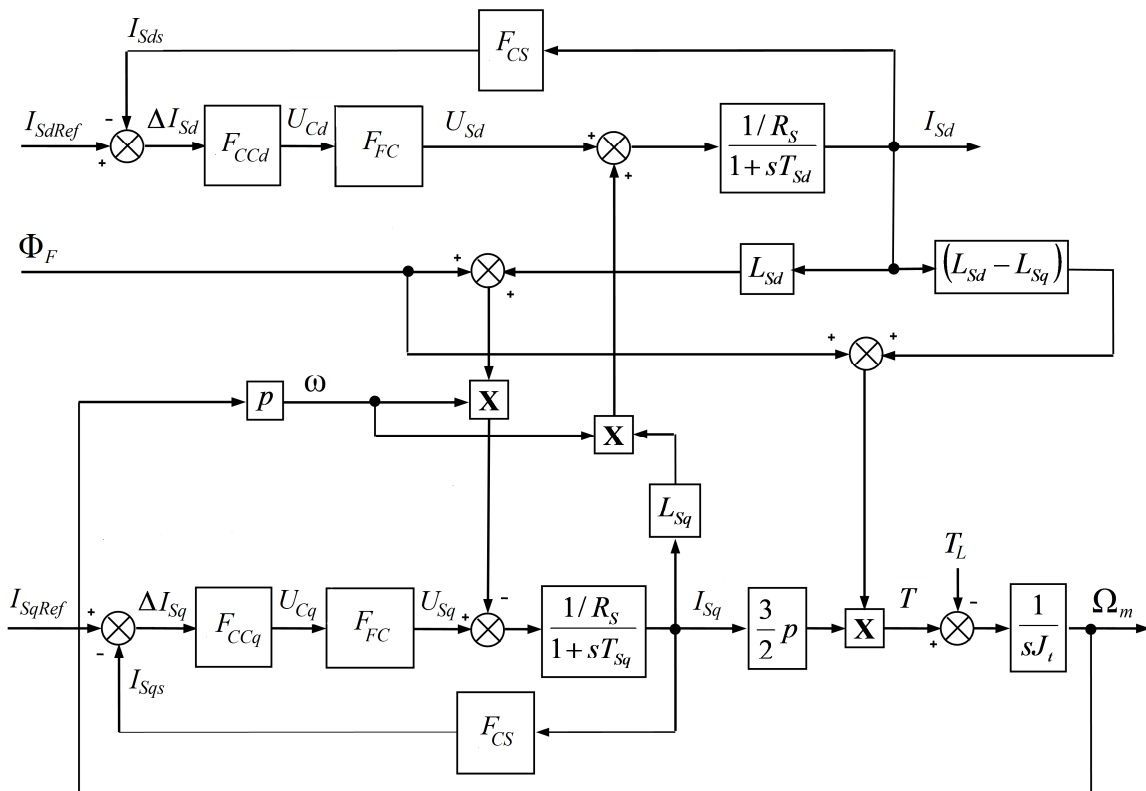| Symbol	Quantity	Value
P_N	nominal power	2.29 kW
T_N	nominal torque	7.3 Nm
n_N	nominal speed	3000 rpm at f=200 Hz
n_{MAX}	maximal speed	7200 rpm
U_{iRMS}	induced line-to-line voltage	263 V at 3000 rpm
I_{SN}	nominal stator current	5.6 A
Φ_F	magnetic flux of the PM	0.1706 Wb
P	number of pole pairs	4
R_S	stator resistance R_S	0.65 Ω
$L_{Sd} = L_{Sq} = L_S$	stator inductance	7.7 mH
J_m	motor inertia	0.00151 kgm²

Figure 3. Speed control structure of the vector controlled AC drive with the PMSM

The PMSM was supplied by a frequency converter (FC) with the DC link voltage $U_d = 200$ V. The control of the FC output voltage is performed by means of a sine PWM with the frequency $f_p = 10$ kHz and the voltage $U_{pmax} = \pm 1$ V.

The transfer function of the frequency converter is indicated as F_{FC} in Eq. (14.). The gain and the time constant of the FC are $K_{FC} = 100$, and $T_{FC} = 0.05$ ms, respectively.

The current sensor is described by the transfer function F_{CS} in Eq. (14). The gain and the time constant of the current sensor are $K_{CS} = 1$ A/A, and $T_C = 0.025$ ms, respectively.

The current controller in the q-axis is described by the transfer function F_{CCq} in Eq. (14). The gain and the time constant of the current controller are $K_{CCq} = 0.609$, and $T_{CCq} = 11.8$ ms, respectively. The current controller parameters were obtained by the optimal modulus method.

The rotor speed and position are measured using the incremental sensor IRC 2048 with the four times multiplication of pulses. The resulting number of pulses is 8192 per revolution. The sampling period is $T_v = 5$ ms.

The time constant of the speed sensor is $T_{SS} = 2.5$ ms. The speed sensor gain K_{SS} is not reflected in the following calculations. The transfer function of the speed sensor is indicated as F_{SS} in Eq. (20).

For the analysis, a regime with the nominal excitation of the steady-state PMSM at nominal speed and therefore at $i_{Sd} = i_{SdRef} = 0$ is considered. The influence of the load torque T_L is neglected.

V. TORQUE CURRENT COMPONENT CONTROL WITHOUT DECOUPLING

The disadvantage of the control structures in Figs. 4 and 5 is that they exhibit the current control deviation (control error) from the viewpoint of the control variable, i.e. the reference current.
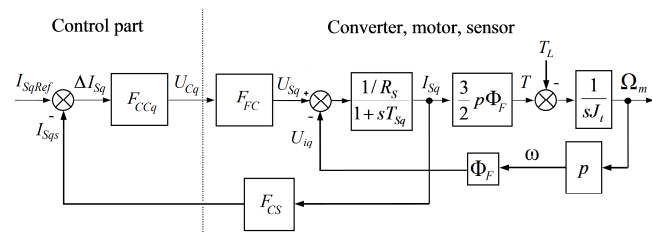

Figure 4. Block scheme of the torque current component control without decoupling

The size of this error is given by (13), which is calculated for the listed value of the total moment of inertia $J_t = 31.1 \cdot 10^{-4}$ kgm^2. According to Eqs. (23) and (24) the current control error is increasing at the smaller value of the inertia (Chapter VI).
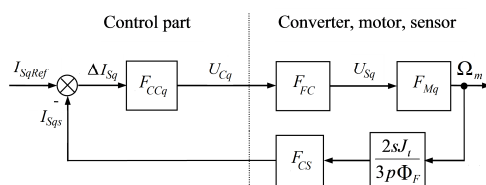

Figure 5. Adjusted block scheme of the torque current component control without decoupling

The steady-state control error is calculated by:

$$\Delta I_{Sq\infty} = \lim_{s \to 0} \left(s \frac{1}{(1 + F_0)} \frac{I_{SqRef}}{s} \right) = \frac{1}{1 + K_0} I_{SqRef} =$$

$$= \frac{1}{1 + 22.98} I_{SqRef} = 0.0417 \, I_{SqRef} \quad . \tag{13}$$

As it can be observed in (13), for the considered parameters, the relative steady-state error is 4.17 %.

According to Fig. 5, the transfer function of the open control loop for the torque current component is described by:

$$F_0 = \frac{I_{Sqs}}{\Delta I_{Sq}} = F_{CCq} F_{FC} F_{Mq} \frac{sJ_t}{(3/2) p \, \Phi_F} F_{CS} \quad , \tag{14}$$

$$F_0 = K_{CCq} \frac{(1 + sT_{CCq})}{sT_{CCq}} \frac{K_{FC}}{(1 + sT_{FC})} \cdot$$

$$\cdot \frac{1/(p \, \Phi_F)}{(1 + sT_m + s^2 T_m T_S)} \frac{s \, J_t}{(3/2) p \, \Phi_F} \frac{K_{CS}}{(1 + sT_{CS})} = \tag{15}$$

$$= K_0 \frac{(1 + sT_{CCq})}{(1 + sT_{FC})(1 + sT_m + s^2 T_m T_S)(1 + sT_{CS})} \quad .$$

$$K_0 = \frac{K_{CCq} K_{FC} J_t K_{CS}}{T_{CCq} (3/2)(p \, \Phi_F)^2} =$$

$$= \frac{0.609 \cdot 100 \cdot 31.1 \cdot 10^{-4} \cdot 1}{0.0118 \cdot (3/2) \cdot (4 \cdot 0.1706)^2} = 22.98 \quad . \tag{16}$$

In Eq. (14), the term F_{Mq} represents the transfer function of the PMSM in the q-axis, defined as:

$$F_{Mq} = \frac{\Omega_m}{U_{Sq}} = \frac{1/(p \, \Phi_F)}{(1 + sT_m + s^2 T_m T_S)} \quad . \tag{17}$$

In Eq. (17), the term T_m can be regarded as a mechanical time constant and the term T_S can be regarded as an electromagnetic motor time constant.

$$T_m = \frac{2 J_t R_S}{3 p^2 \Phi_F^2} = \frac{2 \cdot 31.1 \cdot 10^{-4} \cdot 0.65}{3 \cdot 4^2 \cdot 0.1706^2} = 0.0029 \text{ s} \quad . \tag{18}$$

$$T_S = \frac{L_S}{R_S} = \frac{0.0077}{0.65} = 0.0119 \text{ s} \quad . \tag{19}$$

VI. TORQUE CURRENT COMPONENT CONTROL WITH DECOUPLING

The block scheme and the adjusted block scheme of the torque current component control with decoupling are shown in Figs. 6 and 7.
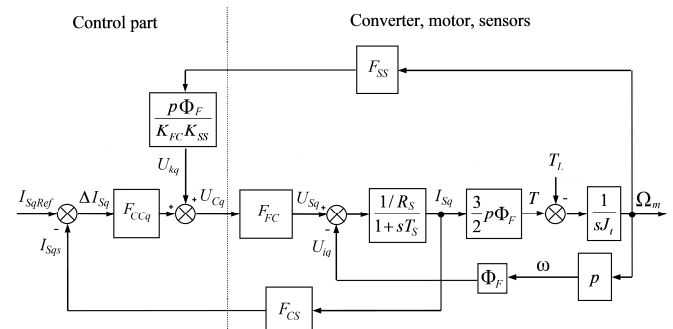

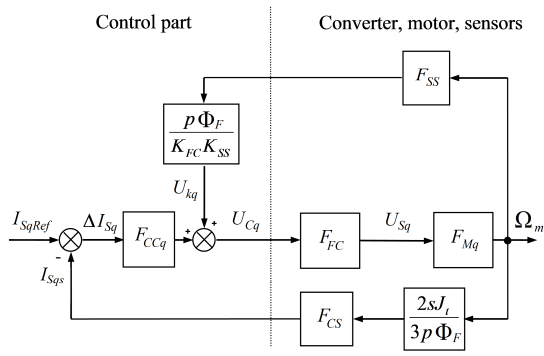Figure 6. Block scheme of the torque current component control with decoupling

Figure 7. Adjusted block scheme of the torque current component control with decoupling

The transfer function of the open control loop with the decoupling according to Figs. 6 and Fig. 7 is defined by:

$$F_0 = \frac{I_{Sqs}}{\Delta I_{Sq}} = \frac{I_{Sqs}}{I_{SqRef} - I_{Sqs}} =$$
$$= F_{CCq} \frac{F_{FC} F_{Mq}}{\left(1 - \frac{F_{FC} F_{Mq} F_{SS} p\,\Phi_F}{K_{SS} K_{FC}}\right)} \frac{s J_t}{(3/2)\,p\,\Phi_F} F_{CS} , \quad (20)$$

In Eq. (21), the term T_m can be regarded as a mechanical time constant.

$$F_0 = K_{CCq} \frac{\left(1 + s T_{CCq}\right)}{s T_{CCq}} \cdot$$

$$\cdot \frac{\dfrac{K_{FC}}{\left(1 + s T_{FC}\right)} \dfrac{1/\left(p\,\Phi_F\right)}{\left(1 + s T_m + s^2 T_m T_S\right)}}{\left(1 - \dfrac{K_{FC}}{\left(1 + s T_{FC}\right)} \dfrac{1/\left(p\,\Phi_F\right)}{\left(1 + s T_m + s^2 T_m T_S\right)} \dfrac{K_{SS}}{\left(1 + s T_{SS}\right)} \dfrac{p\,\Phi_F}{K_{SS} K_{FC}}\right)} \cdot$$

$$\cdot \frac{s J_t}{(3/2)\,p\,\Phi_F} \frac{K_{CS}}{\left(1 + s T_{CS}\right)} \quad .$$

$$(21)$$

The steady-state error at the step of the reference value i_{SqRef} is defined as follows:

$$\Delta I_{Sq\infty} = \lim_{s \to 0}\left(s \frac{1}{\left(1 + F_0\right)} \frac{I_{SqRef}}{s} \right) = 0 . \quad (22)$$

It can be seen, that at steady-state, the error is zero.

VII. SIMULATION RESULTS

The structures of the variable speed electric drives are very complex, therefore it is very suitable to use appropriate simulation tools for verifying these structures. According to the block schemes in Figs. 4 and 6, respectively, we created MATLAB-Simulink simulation structures.

Figs. 8 and 9 show simulated waveforms of the reference torque current component, actual torque current component, and PMSM speed. These simulated waveforms confirm the derived control deviations mentioned in Chapter V. For example in simulation, the steady-state control error of the torque current component is $\Delta I_{Sq\infty} = 0.0838$ A at inertia $J_t = 0.00311$ kgm^2. According to Eq. (13), the steady-state control error is $\Delta I_{Sq\infty} = 0.0834$ A.

The waveforms of the actual torque current component i_{Sq}

were obtained from the control structure without decoupling (Figs. 8 and 9) and with decoupling (Figs. 10 and 11) at the step of the reference torque current $i_{SqRef} = 2$ A.

The control structure without decoupling gives at steady-state, for the lower inertia $J_t = J_m = 0.00151$ kgm^2 (Fig. 8), the relative error:

$$\delta_{Isq} = \frac{\Delta I_{Sq\infty}}{I_{SqRef}} 100 = \frac{2 - 1.8349}{2} 100 = 8.26 \text{ \%} , \quad (23)$$
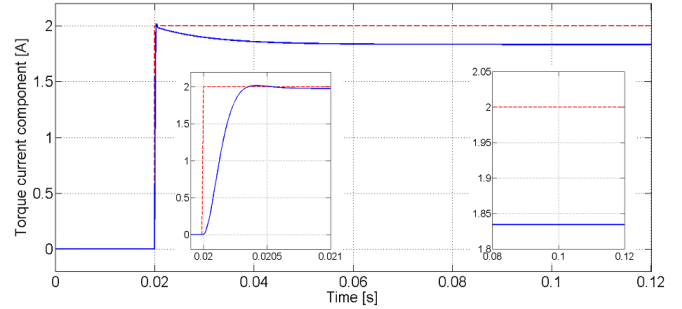
what is in accordance with Eq. (13).

Figure 8. Reference (red) and actual (blue) torque current component without decoupling, with inertia of $J_t = J_m = 0.00151$ kgm^2, and steady-state value of torque current component of 1.8349 A.
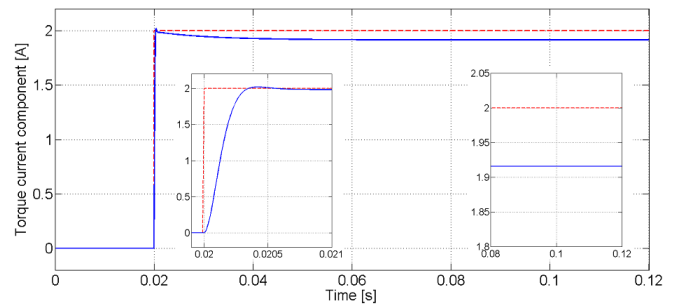

Figure 9. Reference (red) and actual (blue) torque current components without decoupling, with inertia of $J_t = 0.00311$ kgm^2, and steady-state value of the torque current component of 1.9162 A.

The control structure without decoupling gives at steady-state, for inertia $J_t = 0.00311$ kgm^2 (Fig. 9), the relative error:

$$\delta_{Isq} = \frac{\Delta I_{Sq\infty}}{I_{SqRef}} 100 = \frac{2 - 1.9162}{2} 100 = 4.19 \text{ \%} , \quad (24)$$

what is in accordance with Eqs. (13) and (15).

The small difference appears since in steady-state, the simulated waveform of the torque current component i_{Sq} is not still.

According to Eq. (15), for the reduced value of inertia, it is possible to obtain the open loop gain of $K_0 = 11.16$ against to the original value $K_0 = 22.98$. In this case, according to Eq. (13), at steady-state, the error is defined by:

$$\Delta I_{Sq\infty} = \frac{1}{1 + K_0} I_{SqRef} =$$
$$(25)$$
$$= \frac{1}{1 + 11.16} I_{SqRef} = 0.08225 I_{SqRef} .$$

According to Eq. (25), at steady state, the relative error is 8.22%.

At the control structure with decoupling, at steady-state the relative error is equal zero (Fig. 10), that is in accordance with Eq. (22). For the lower value of inertia $J_t = J_m = 0.00151$ kgm^2, the differences are not so evident as

for the structure without decoupling.

Figs. 11 and 12 show the waveforms of the speed during acceleration of the AC drive with the currents as is shown in Fig. 8 - Fig. 10 without load.

The details plotted in Fig. 8 - 12 confirm the mentioned theoretical assumptions. It is obvious that the vector controlled AC drive with the decoupling has better dynamics, i.e. faster speed growth.
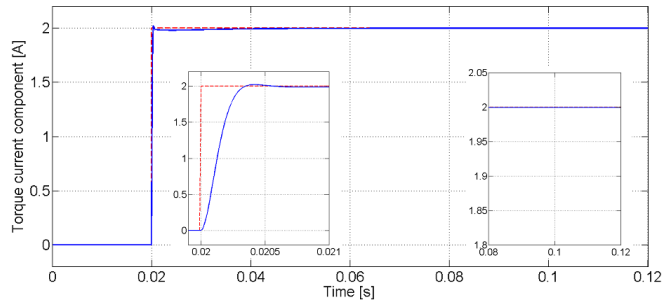

Figure 10. Reference (red) and actual (blue) torque current component with decoupling, with inertia of $J_t = 0.00311$ kgm^2, and steady-state value of the torque current component of 2.0 A.
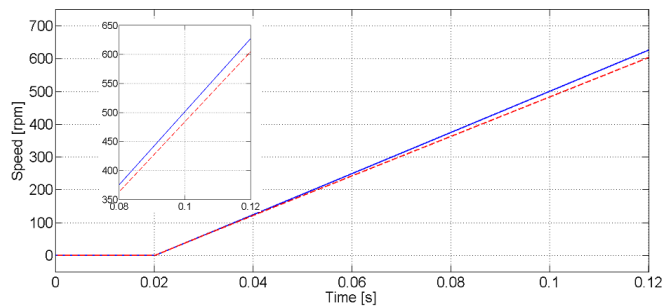

Figure 11. PMSM speed for the torque current component without decoupling (red) and with decoupling (blue), with inertia of $J_t = 0.00311$ kgm^2.
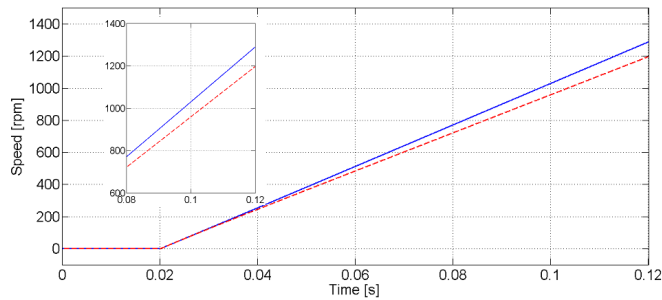

Figure 12. PMSM speed for the torque current component without decoupling (red) and with decoupling (blue), with inertia of $J_t = J_M = 0.00151$ kgm^2.

VIII. EXPERIMENTAL RESULTS

For the experimental verification of the steady-state deviation of the torque current component in the structure of the vector controlled PMSM, experimental measurements were performed on the PMSM drive from the laboratory of the Department of Electronics, VSB - Technical University of Ostrava, with a PMSM type 1FK 7063-5AF71 (Siemens). The PMSM was connected with an induction machine as load, which increases the moment of inertia of the whole set (Fig. 13).

The PMSM parameters used in the simulation correspond to these of the real PMSM drive (Chapter IV). The PMSM was powered by a frequency converter that consists of a rectifier, voltage DC link and a voltage source inverter. The

control system contains a TMS320F28335 DSP.

The algorithm including the stator currents and DC-link voltage measuring is processed with the sampling period of 50 μs.

Figs. 16 and 17 show waveforms of selected quantities during the start-up of the PMSM drive to speed 600 rpm without decoupling (Fig. 16) and with decoupling (Fig. 17). The PMSM drive is without load.
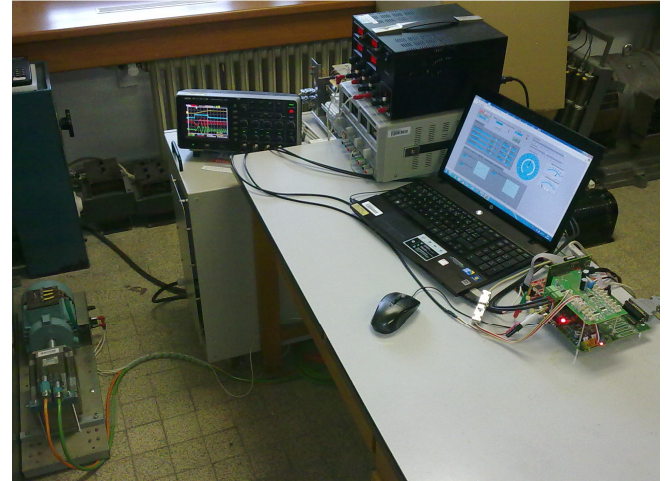

Figure 13. Experimental installation at the laboratory of the Department of Electronics, VSB - Technical University of Ostrava.
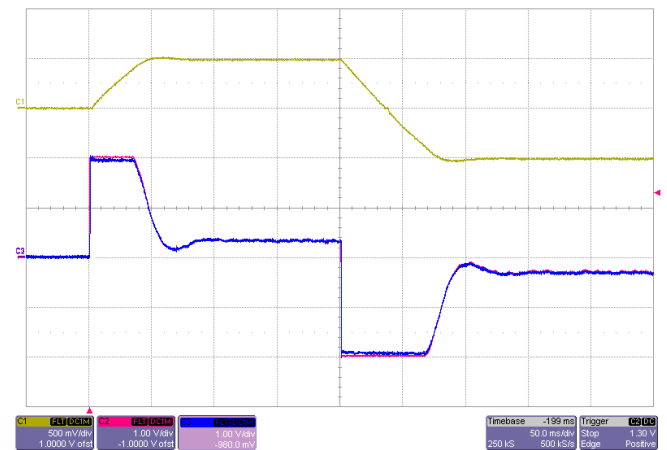

Figure 14. PMSM speed (yellow), the reference (red) and actual (blue) torque producing stator current without decoupling, with inertia of $J_t = 0.00311$ kgm^2 (current scale 1 A/div, speed scale 500 rpm/div, time scale 50 ms/div).

Figure 15. PMSM speed (yellow), the reference (red) and actual (blue) torque producing stator current with decoupling, with inertia of $J_t = 0.00311$ kgm^2 (current scale 1 A/div, speed scale 500 rpm/div, time scale 50 ms/div).
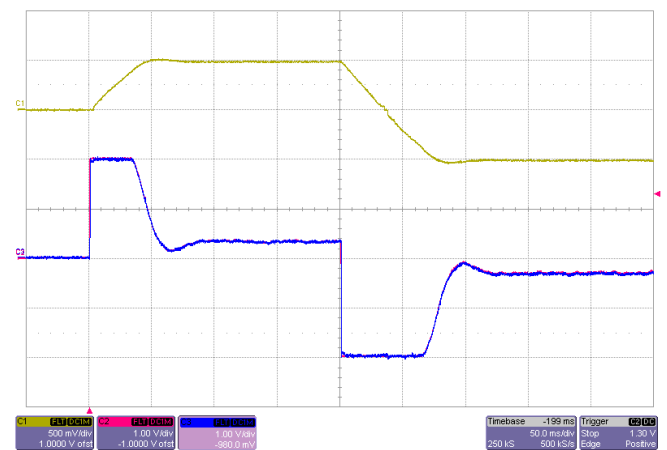
Figure 16. PMSM speed (yellow), the reference (red) and actual (blue) torque producing stator current without decoupling, with inertia of J_t = 0.00311 kgm^2 (current scale 0.5 A/div, speed scale 500 rpm/div, time scale 10 ms/div).

Figure 17. PMSM speed (yellow), the reference (red) and actual (blue) torque producing stator current with decoupling, with inertia of J_t = 0.00311 kgm^2 (current scale 0.5 A/div, speed scale 500 rpm/div, time scale 10 ms/div).

In Figs. 14 and 16, the steady-state control error of the torque current component is presented. The reference value of the torque current component is 2 A and the steady-state value of the torque current component is 1.9 A.

In Figs. 15 and 17, it can be seen that the reference and the steady-state values of the torque current component are both 2 A.

Figure 18. PMSM speed without decoupling (above) and with decoupling (below), total moment of inertia J_t = 0.00311 kgm^2 (speed scale 500 rpm/div, time scale 10 ms/div).

Fig. 18 shows the speed responses of the PMSM drive at start-up. A time difference of 6 ms speed rise time between the control structure without decoupling and those with decoupling can be observed.

IX. CONCLUSION

The described analysis demonstrates that at steady-state the error of the torque component of the stator current vector is eliminated by involving correction decoupling circuits. This fact was derived in (22) and verified by the simulation and experimental results.

However, the practical accuracy depends on settings in the control block. Deviations could occur due to change in the gain of the frequency converter.

For the control structure without decoupling circuits, the steady state error greatly depends on system and controller parameters, as it can be seen on Eqs. (13) and (15).

If the PMSM drive works in the field weakening mode, where the magnetizing current is decreased from zero to negative values, it is necessary to carry out a gain adaptation in the decoupling circuit with respect to the change of the magnetizing current component.

The above-mentioned conclusions, with some modifications, are also valid for other AC drives with vector control or with similar quality control and of course for DC drives.

Measured experimental waveforms confirmed the theoretical assumptions and the simulation results. In the case of the control structure without decoupling circuit, when the inertia is 0.00311 kgm^2, the steady state value of the torque current component was of 1.9162 A in simulation and 1.9 A in the experiment. In the case of the control structure with decoupling circuit, at steady-state, the current error is zero in both cases, simulation and experiment.

REFERENCES

[1] F.J. Gieras and M. Wing, Permanent magnet motor technology: Design and applications. Third Edition, CRC Press, 2010.
[2] N. Bernard, F. Martin, and M.E.H. Zaïm, "Design methodology of a permanent magnet synchronous machine for a screwdriver application," IEEE Transactions on Energy Conversion, vol. 27, no. 3, pp. 624-633, Sept. 2012. doi: 10.1109/TEC.2012.2199494
[3] J. Soleimani, M.B. Bafghi, and M. Shojaeepoor, "IPM synchronous motor for traction applications: performance analysis considering hysteresis loop characteristics variation," International Review of Electrical Engineering - IREE, vol.7, no.1, pp. 3297-3303, 2012.
[4] C.H. Lin, "Hybrid recurrent wavelet neural network control of PMSM servo-drive system for electric scooter," International Journal of Control Automation and Systems, vol. 12, no. 1, pp. 177-187, 2014. doi: 10.1007/s12555-012-0190-2
[5] T. Tudorache and M. Popescu, "Optimal Design Solutions for Permanent Magnet Synchronous Machines," Advances in Electrical and Computer Engineering, vol.11, no. 4, pp. 77-82, 2011. doi: 10.4316/ AECE. 2011.04012
[6] J. Vittek, V. Vavrus, P. Bris, and L. Gorel, "Forced dynamics control of the elastic joint drive with single rotor position sensor," Automatika, vol. 54, no. 3, pp. 337-347, 2013. doi: 10.7305/ automatika.54-3.160
[7] Y.A.R.I. Mohamed, and T.K. Lee, "Adaptive self-tuning MTPA vector controller for IPMSM drive system," IEEE Transactions on Energy Conversion, vol. 21, no. 3, pp. 636-644, Sept. 2006. doi: 10.1109/TEC.2006.878243
[8] M. Moujahed, H. Ben Azza, M. Jemli, and M. Boussak, "Speed estimation by using EKF techniques for sensor-less DTC of PMSM with load torque observer," International Review of Electrical Engineering - IREE, vol. 9, no. 2, pp. 270-279, 2014.
[9] P. Chlebis, P. Vaculik, P. Moravcik, and Z. Pfof, "Direct torque control methods for three-level voltage inverter," in Proc. 10th Int. Scientific Conf. on Electric Power Engineering 2009, Kouty nad Desnou, Czech Republic, 2009, pp. 352-356.
[10] T.D. Do, H.H. Choi, and J.W. Jung, "Nonlinear Optimal DTC Design and Stability Analysis for Interior Permanent Magnet Synchronous Motor Drives," IEEE/ASME Transactions on Mechatronics, vol. 20, no. 6, pp. 2716-2725, Dec. 2015. doi: 10.1109/TMECH.2015. 2426725
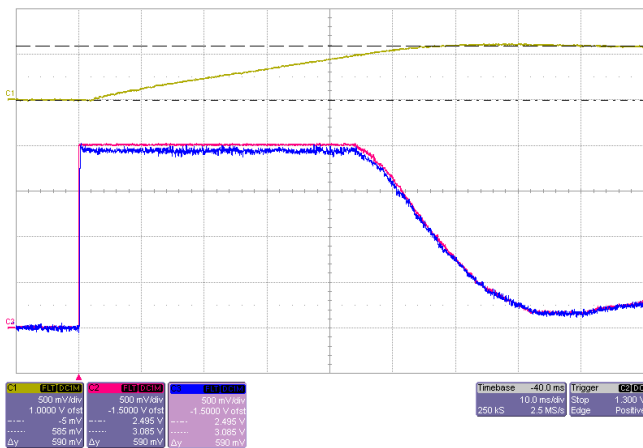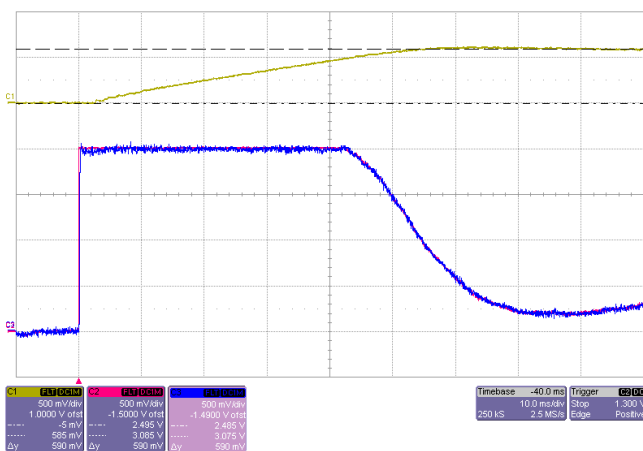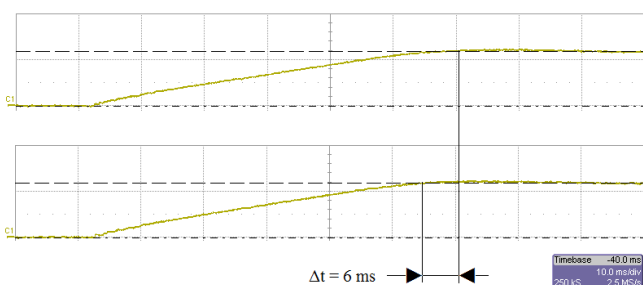
[11] C. Calleja, A. López-de-Heredia, H. Gaztañaga, L. Aldasoro, and T. Nieva, "Validation of a Modified Direct-Self-Control Strategy for PMSM in Railway-Traction Applications," IEEE Transactions on Industrial Electronics, vol. 63, no. 8, pp. 5143-5155, Aug. 2016. doi: 10.1109/TIE.2016.2572661

[12] F. Niu, K. Li, and Y. Wang, "Direct torque control for permanent-magnet synchronous machines based on duty ratio modulation," IEEE Transactions on Industrial Electronics, vol. 62, no. 10, pp. 6160-6170, Oct. 2015. doi: 10.1109/TIE.2015.2426678

[13] M. Gecic, M. Kapetina, and D. Marcetic, "Energy Efficient Control of High Speed IPMSM Drives - A Generalized PSO Approach," Advances in Electrical and Computer Engineering, vol.16, no. 1, pp. 27-34, 2016. doi: 10.4316/AECE.2016.01004

[14] G. Haines and N. Ertugrul, "Wide Speed Range Sensorless Operation of Brushless Permanent-Magnet Motor Using Flux Linkage Increment," IEEE Transactions on Industrial Electronics, vol. 63, no. 7, pp. 4052-4060, July 2016. doi: 10.1109/TIE.2016.2544250

[15] M. Seilmeier and B. Piepenbreier, "Sensorless control of PMSM for the whole speed range using two-degree-of-freedom current control and hf test current injection for low-speed range," IEEE Transactions on Power Electronics, vol. 30, no. 8, pp. 4394-4403, 2015. doi: 10.1109/TPEL.2014.2353215

[16] G.F.H. Beng, X. Zhang, and D.M. Vilathgamuwa, "Sensor Fault-Resilient Control of Interior Permanent-Magnet Synchronous Motor Drives," IEEE/ASME Transactions on Mechatronics, vol. 20, no. 2, pp. 855-864, April 2015. doi: 10.1109/TMECH.2014.2311126

[17] J. Kim, I. Jeong, K. Nam, J. Yang, and T. Hwang, "Sensorless control of PMSM in a high-speed region considering iron loss," IEEE Transactions on Industrial Electronics, vol. 62, no. 10, pp. 6151-6159, Oct. 2015. doi: 10.1109/TIE.2015.2432104

[18] D. Vosmik and Z. Peroutka, "Sensorless control of permanent magnet synchronous motor employing extended Kalman filter in combination with hf injection method," in Proc. 14th European Conf. on Power Electronics and Applications, Birmingham, England, 2011, pp. 1-10.

[19] G. Luo, R. Zhang, Z. Chen, W. Tu, S. Zhang, and R. Kennel, "A Novel Nonlinear Modeling Method for Permanent-Magnet Synchronous Motors," IEEE Transactions on Industrial Electronics, vol. 63, no. 10, pp. 6490-6498, Oct. 2016. doi: 10.1109/TIE.2016. 2578839

[20] S. Lee, Y.S. Jeong, Y.J. Kim, and S.Y. Jung, "Novel analysis and design methodology of interior permanent-magnet synchronous motor using newly adopted synthetic flux linkage," IEEE Transactions on Industrial Electronics, vol. 58, no. 9, pp. 3806-3814, Sept. 2011. doi: 10.1109/TIE.2010.2093479

[21] S. Li, L. Harnefors, M. Iwasaki, "Modeling, Analysis, and Advanced Control in Motion Control Systems-Part II," IEEE Transactions on Industrial Electronics, vol. 63, no. 10, pp. 6371-6374, Oct. 2016. doi: 10.1109/TIE.2016.2597132

[22] J.S. Lee and R.D. Lorenz, "Robustness Analysis of Deadbeat-Direct Torque and Flux Control for IPMSM Drives," IEEE Transactions on Industrial Electronics, vol. 63, no. 5, pp. 2775-2784, May 2016. doi: 10.1109/TIE.2016.2521353

[23] J.A. Güemes, A.M. Iraolagoitia, J.I. Del Hoyo, and P. Fernández, "Torque analysis in permanent-magnet synchronous motors: A comparative study," IEEE Transactions on Energy Conversion, vol. 26, no. 1, pp. 55-63, March 2011. doi: 10.1109/TEC.2010.2053374

[24] M. Frivaldsky, P. Drgona, and P. Spanik, "Experimental analysis and optimization of key parameters of ZVS mode and its application in the proposed LLC converter designed for distributed power system application," International Journal of Electrical Power & Energy Systems, Vol. 47, pp. 448-456, May 2013. doi: 10.1016/j.ijepes.2012. 11.016

[25] T. Tudorache, I. Trifu, C. Ghita, and V. Bostan, "Improved mathematical model of PMSM taking into account cogging torque oscillations," Advances in Electrical and Computer Engineering, vol.12, no. 3, pp. 59-64, 2012. doi: 10.4316/AECE.2012.03009

[26] C.K. Lin, T.H. Liu, J.T. Yu, L.C. Fu, and C.F. Hsiao, "Model-free predictive current control for interior permanent-magnet synchronous motor drives based on current difference detection technique," IEEE Transactions on Industrial Electronics, vol. 61, no. 2, pp. 667-681, Feb. 2014. doi: 10.1109/TIE.2013.2253065

[27] F.I. Bakhsh, M. Khursheed, S. Ahmad, and A. Iqbal, "A novel technique for the design of controller of a vector-controlled permanent magnet synchronous motor drive," in Proc. 2011 Annual IEEE India Conference - INDICON, Hyderabad, India, 2011, pp. 1-6. doi: 10.1109/INDCON.2011.6139558

[28] J. Kim, I. Jeong, K. Lee, and K. Nam, "Fluctuating current control method for a PMSM along constant torque contours," IEEE Transactions on Power Electronics, vol. 29, no.11, pp. 6064-6073, Nov. 2014. doi: 10.1109/TPEL.2014.2299548

[29] T. Tudorache, M. Modreanu, "Design Solutions for Reducing the Cogging Torque of PMSM," Advances in Electrical and Computer Engineering, vol.13, no. 3, pp. 59-64, 2013. doi: 10.4316/AECE.2013. 03010

[30] M.H. Vafaie, B. Mirzaeian Dehkordi, P. Moallem, and A. Kiyoumarsi, "Minimizing Torque and Flux Ripples and Improving Dynamic Response of PMSM Using a Voltage Vector With Optimal Parameters," IEEE Transactions on Industrial Electronics, vol. 63, no. 6, pp. 3876-3888, June 2016. doi: 10.1109/TIE.2015.2497251